Photocatalytic activity of TiO2-WO3 mixed oxides in formic acid oxidation

Photocatalytic activity in oxidation and reduction reactions of TiO_2-WO_3 mixed oxides

Francesca Riboni[a], Maria Vittoria Dozzi[a], Maria Cristina Paganini[b], Elio Giamello[b], Elena Selli[a,*]

Dipartimento di Chimica, Università degli Studi di Milano, Via Golgi 19, I-20133 Milano, Italy

[b] *Dipartimento di Chimica, Via Giuria 7, 10125 Torino, Italy*

A B S T R A C T

TiO_2 and Ti-W mixed oxide photocatalysts, with W/Ti molar ratios in the 0 – 5% range, were prepared through a simple sol-gel method, followed by annealing at 500 or 700 °C, and their photo-activity was tested in (*i*) a down-hill process, i.e. the photo-oxidation of formic acid performed in the aqueous phase under ambient *aerobic* conditions, and (*ii*) an up-hill reaction, i.e. H_2 production through methanol photo-steam reforming performed under *anaerobic* conditions. XRPD and BET analyses evidenced that full anatase materials were obtained in the presence of tungsten, even after calcination at 700 °C, with a progressively increased surface area and smaller particles dimensions. Tungsten can both enter the titania lattice, as demonstrated by HAADF-STEM analysis, and possibly segregate as amorphous WO_3 on the photocatalysts surface. Best performing photocatalysts in both investigated reactions was that containing 1.0 mol% W/Ti, taking advantage of the high surface area and full anatase structure of these mixed oxide materials, even if calcined at 700 °C, whereas electron transfer from TiO_2 to WO_3 leading to increased electron-hole separation, appears to have no beneficial effects in the investigated reactions, most probably due to the lower energy level of the WO_3 conduction band.

[*] Corresponding author at: Dipartimento di Chimica, Università degli Studi di Milano, via Golgi 19, I-20133 Milano, Italy. Tel.: +39 02 503 14237; fax: +39 02 503 14300.

E-mail address: elena.selli@unimi.it (E. Selli).

1. Introduction

Photocatalysis represents a powerful tool to exploit the energy associated with light in a number of different applications, including pollutants removal from water and air for environmental remediation and solar into chemical energy conversion to produce so-called solar fuels. The key advantages of the use of TiO_2 as photocatalyst over other semiconductor oxides are well established and enormous efforts have been directed in recent years to improve its performance by reducing the intrinsic limitations in its use as photocatalyst. These mainly consist in its relatively large band gap (3.0 – 3.2 eV), that limits the use of sunlight to promote photocatalytic reactions, in the low rate of electron transfer to reducible species and in the high rate of photoproduced electron-hole pairs recombination. The generation of long-living and spatially separated charge carriers thus appears a primary goal to be achieved. Combining TiO_2 with another semiconductor with suitable band gap and band edge values is one of the strategies so far explored for this aim [1-6].

In a composite photocatalytic system, consisting of two (or more [7]) semiconductor materials in intimate contact, the heterojunction formed at their interface generates a multicomponent tandem structure which promotes the generation and mobility of the charge carriers, and thus improves the photocatalytic activity. Owing to the availability of a large number of semiconducting materials with different band gap and band offsets, the composition of a semiconductor composite can be conveniently designed to meet the energetic requirements of specific photocatalytic reactions. For instance, among the many examples that can be found in the literature, Nb_2O_5/TiO_2 composites, featuring reduced rate of electron-hole recombination compared to pure TiO_2, have been investigated in the photocatalytic degradation of alcohols [8]. In combination with cerium oxide, TiO_2 has been shown to stabilize the Ce(III) oxidation state, which guarantees higher photoactivity of the CeO_x/TiO_2 composite materials. Indeed, Ce^{3+}

centers and the concomitant formation of oxygen vacancies within the CeO_x/TiO_2 structure act as hole acceptors and reduce the probability of electron-hole recombination [9]. Also TiO_2/WO_3 mixed oxides have been shown to exhibit higher photoactivity with respect to that of both single oxide components [3,5,6]. From the mechanistic point of view, the electrons photopromoted in the TiO_2 conduction band (CB) are expected to transfer to the CB of WO_3, while the holes remain more likely trapped in the valence band (VB) of titania. The so obtained spatial separation between electrons and holes reduces their recombination probability, increases the electron lifetime and enhances the photoactivity performance of TiO_2/WO_3 mixed oxides [3,5,6].

In the present work, we investigate the effects of different amounts of WO_3 (W/Ti = 1 – 5 mol%) and different annealing temperatures (500 and 700 °C) on the photocatalytic activity of a series of TiO_2/WO_3 composite materials. Both a thermodynamically down-hill reaction performed under *aerobic* conditions, i.e. the photomineralization of formic acid in aqueous suspension, and an up-hill reaction performed under *anaerobic* conditions, i.e. H_2 production by methanol photosteam reforming, were employed as photoactivity test reactions. In a recent study [6] we evidenced that for TiO_2-WO_3 mixed oxide materials, prepared by a sol-gel synthesis starting from organic precursors and calcined at 700 °C, an optimal tungsten content maximizes photoactivity in both an aqueous phase and a gas phase photocatalytic oxidation reaction. However the question remained open whether the beneficial effect on photoactivity of small amounts of tungsten might be associated to the presence of WO_3 domains within the TiO_2 structure, favoring the separation of photoproduced electron-hole couples, or to other tungsten-induced effects on the surface and bulk properties of titania.

2. Experimental

2.1. Photocatalysts preparation

Titanium(IV) isopropoxide ($Ti(OCH(CH_3)_2)_4$, Sigma-Aldrich, 97%) and tungsten(VI) hexa-ethoxide ($W(OC_2H_5)_6$, Alfa-Aesar, 99.8% (metal basis), 5 wt.% in ethanol) were used as titanium and tungsten precursors, respectively, for the synthesis of TiO_2-WO_3 mixed oxide photocatalysts, according to the already detailed procedure [6]. Briefly, anhydrous ethanol was employed as solvent of solutions containing the titanium and tungsten precursors in appropriate amount so as to produce mixed oxide samples with nominal W/Ti molar ratios equal to 1.0, 3.0 and 5.0%. Water was then added dropwise under vigorous stirring at 30 °C, so as to obtain a low-titanium-to-water molar ratio, favoring the formation of metal oxide nanoparticles [10]. The white slurry obtained after concentration under reduced pressure was kept in oven at 70°C overnight and finally annealed either at 500 or at 700 °C under a 100 mL min^{-1} air flow, for 4 h. Also pure TiO_2 powders were synthesized and annealed under identical conditions, without adding the tungsten precursor. The samples were labeled TW*x*_*y*, with *x* referring to the W/Ti molar ratio (0 – 5%) and *y* to the annealing temperature in Celsius (500 or 700 °C).

2.2. Photocatalysts characterization

XRPD patterns were recorded with a Phillips PW3020 powder diffractometer, operating at 40 kV and 40 mA, using Cu Kα (λ = 1.54056 Å) as X-ray source. The diffractograms were recorded by continuous scanning in the 2θ-range = 20 – 80°, with a 0.05° step. Quantitative phase analysis was carried out with the Rietveld refinement method and the average crystallite size was determined by applying the Scherrer equation to the main anatase reflection (peak at 2θ = 25.5°, corresponding to the (1 0 1) crystal plane).

The BET surface area of each sample was determined by N_2 adsorption in a Micrometrics Tristar 3000 apparatus at 77 K, after outgassing the samples at 300 °C for 4 h. The absorption properties of the powders were determined by means of a UV-visible reflectance

spectrophotometer (Jasco, V-650), equipped with an integrating sphere. Ba_2SO_4 was adopted as reference material.

The High-Angle Annular Dark-Field Scanning Transmission Electron Microscopy (HAADF-STEM) images were recorded with an aberration-corrected HD-2700CS Hitachi STEM microscope, operated at an acceleration potential of 200 kV. A few drops of each powder suspended in ethanol were deposited on a perforated carbon foil, supported on a copper grid. After drying, the grid was mounted on the single tilt holder of the microscope.

Electron Paramagnetic Resonance (EPR) spectra were recorded by means of a Bruker EMX spectrometer with cylindrical cavity, operating at 100 kHz field modulation. Experiments were performed at 77 K, either in the dark or under UV irradiation.

2.3. Photocatalytic activity tests

Formic acid (FA) photodegradation runs were performed under atmospheric conditions, as already described [11,12], employing a fixed photocatalyst amount (0.1 g L^{-1}) and a fixed initial FA concentration (1.0×10^{-3} mol L^{-1}). Prior to irradiation, the so-formed suspensions were left in the dark for 15 min under stirring, to attain adsorption equilibrium. The commercial lamp (Osram Powerstar HCI-T 150W/NDL) employed as light source mainly emits visible light at wavelength above 400 nm, with a small emission in the 350 – 400 nm range [12] and a full emission intensity on the photoreactor of 2.53×10^{-7} Einstein s^{-1} cm^{-2}. The residual amount of formate anion contained in the samples withdrawn from the photoreactor at different times was determined by ion chromatography with conductivity detection, after centrifugation. All photocatalytic runs were repeated at least twice to check their reproducibility.

H_2 production by methanol photo-steam reforming was performed in a closed stainless steel system. The set-up used in the kinetic runs and the optimized working conditions have been described elsewhere [13,14]. The photocatalyst bed, prepared by depositing a fixed amount of

photocatalyst (14 mg) on 3 g of 20-40 mesh quartz, was inserted in a flat cylindrical photoreactor, with a Pyrex glass window and an irradiated surface of 20 cm^2. The photoreactor was then inserted in the closed stainless steel system and oxygen was removed by purging with nitrogen for 30 min, prior to any run. N_2 was also used as carrier gas during the photoactivity tests. It was continuously fed into the photoreactor at 40 mL min^{-1} constant rate, after having been saturated with water and methanol by bubbling through a 20 vol.% CH_3OH aqueous solution maintained at 30 °C. The photoreactor temperature was also maintained at 30 °C, while the absolute pressure, 1.2 bar at the beginning of the runs, slightly increased during irradiation as a consequence of the accumulation of gas-phase products. The recirculating gas phase was automatically sampled at specific time intervals and analyzed in an Agilent 6890 N gas-chromatograph. An iron halogenide mercury arc lamp (Jelosil, 250 W) emitting in the 330 – 450 nm wavelength range (full intensity of 6.0×10^{-8} Einstein s^{-1} cm^{-2}), was adopted as irradiation source. Typically, runs lasted 6 h and were repeated twice to check their reproducibility.

3. Results and discussion

3.1. Crystal structure and physical properties

Fig. 1(a) shows the XRPD patterns of all synthesized materials. The TW*x*_500 photocatalysts proved to be composed of pure anatase phase, regardless of their W content (0 – 5 mol%). Conversely, among the samples annealed at 700 °C, pure TiO_2 (TW0_700) mainly consisted of rutile phase (90 wt.%), as revealed by the (1 1 0) reflection at $2\theta = 27.4°$ appearing in its XRPD pattern, with a smaller contribution (10 wt.%) arising from anatase ($2\theta = 25.5°$). However, all W-containing photocatalysts of the TW*x*_700 series were composed of pure anatase, demonstrating that small amounts of tungsten (in the 1 – 5 mol% range) completely inhibit the transformation of

the anatase into the rutile phase, typically occurring when annealing TiO_2 at temperature above 600 °C [3,6,15].

As recently pointed out [16], in principle W^{6+} can be easily introduced in the titania lattice and substitute Ti^{4+} cations, due to their very similar ionic radii (ionic radius of W^{6+} = 0.0600 nm, ionic radius of Ti^{4+} = 0.0605 nm [17]). An accurate analysis of the main reflections of the anatase phase reveals that, regardless of the calcination temperature, the anatase reflection peak shifted toward lower 2θ-values with increasing tungsten content (Fig. 1(b)). This observation could be related to the expansion of the anatase cell occurring upon tungsten introduction and proves that a fraction of W can enter the TiO_2 lattice. Moreover, the absence of features attributable to WO_3 in the XRPD patterns of the Ti-W mixed oxides is in line with tungsten ions incorporation into titania, either substituting titanium ions or being located at interstitial sites.

The size of anatase crystallites (d_A) in TiO_2 and TiO_2-WO_3, calculated by applying the Scherrer equation to the XRPD data, are reported in Table 1. While the anatase crystallite size in the TW*x*_500 photocatalyst series was found to be almost independent of the W content, being ca. 6 nm for all specimens, that calculated for pure titania TW0_500 was ca. doubled (13 nm). This is in line with the already reported tungsten ability of inhibiting the anatase crystallite growth [5,6]. Regarding the TW*x*_700 series, the anatase particle size in W-containing samples were found to be smaller than that of pure titania TW0_700 and the calculated d_A values appear to slightly decrease with increasing W amount, as also reported in recent literature [4].

The specific surface area (SSA) values obtained from BET analysis perfectly match the trend of anatase nanoparticle sizes obtained from XRPD analysis. All W-containing samples of the TW*x*_500 series exhibit similar SSA, in line with their comparable nanoparticles size, that of TW0_500 being significantly lower. Finally, the SSA values of the TW*x*_700 series is higher

than that of pure TiO_2 (TW0_700) and monotonically increases as a function of the W/Ti molar ratio.

The absorption spectra of all investigated photocatalysts are shown in Fig. 1(c). All powders exhibit an absorption onset at $\lambda \sim 400$ nm, owing to TiO_2 band gap excitation. Only TW0_700, in line with its high rutile-phase content (Table 1), exhibit a slightly red-shifted absorption threshold ($\lambda \sim 420$ nm). Notably, an absorption shoulder at $\lambda \sim 450$ nm is also observed in the absorption spectrum of TW3_500 and TW5_500. As the absorption threshold of WO_3 is in the 400–450 nm range [18], this might be attributed to the formation of WO_3 surface aggregates.

Tungsten incorporation within TiO_2 was confirmed by HAADF-STEM analysis. As shown in Fig. 2, the images of the TW*x*_500 (*x* = 1, 3 and 5) photocatalyst series highlight the presence of atomically dispersed tungsten, appearing as bright spots due to its Z-contrast in the titania lattice. The tiny light spots represent orderly aligned rows of W atoms incorporated into the TiO_2 matrix. Furthermore, the number of tungsten centers increase with increasing W/Ti nominal molar ratio, leading to a less spread W distribution in the case of TW5_500. The average diameters of the TiO_2 crystallites obtained from STEM analysis were in agreement with those calculated from XRPD data (Table 1).

The chemical composition of both pure TiO_2 and TiO_2-WO_3 composite materials, annealed at either 500 or 700 °C, was investigated through X-ray photoelectron spectroscopy (XPS), as detailed in previous studies [6,19]. Apart from the Ti 2p features, namely Ti $2p_{1/2}$ at binding energy (BE) ~ 465 eV and Ti $2p_{3/2}$ at BE ~ 459 eV, supporting the formation of a titania-based matrix also in TiO_2-WO_3 composite materials, in all W-containing samples the W $4f_{5/2}$ (BE ~ 37.5 eV) and W $4f_{7/2}$ (BE ~ 36 eV) signals appeared, compatible with the formation of tungsten trioxide clusters [20]. In the TW*x*_500 series the intensity of these peaks increased with increasing W/Ti nominal molar ratio, at the expense of the Ti 3p signal, overlapping in the same

BE region, with the W/Ti percent molar ratio obtained by XPS analysis always being slightly above the nominal value [19], whereas no sizeable variation of the W 4f peaks as a function of the W/Ti ratio could be detected for samples annealed at 700 °C [6]. The main O 1s band was always found at BE ~ 530 eV, for either pure TiO_2 or TiO_2-WO_3 mixed oxides, independently of the annealing temperature, and was assigned to the formation of O–Ti bonds in the lattice. Remarkably, the peak at BE ~ 533 eV corresponding to –OH groups on the oxide surface, was almost undetectable in the W-containing samples of the TW*x*_700 series, by virtue of the tungsten ability in reducing titania surface hydration [6]. Thus XPS analysis is compatible with the formation of amorphous WO_3 domains on the photocatalyst surface.

3.2. Formic acid photocatalytic degradation

FA concentration decreased linearly with time under irradiation, as in previous studies [12,21,22]. Thus, the photocatalytic activity of all tested samples can be compared in terms of the zero order rate constants k ($M\ s^{-1}$) shown in Fig. 3(a), which were obtained by fitting the FA concentration vs. time linear decline occurring during the photocatalytic runs. Depending on the temperature of photocatalyst annealing, two photoactivity trends can be distinguished as a function of the W/Ti ratio. Indeed, for the TW*x*_500 photocatalysts series, k values decrease with increasing the W content; hence the most active material is pure titania TW0_500. A similar photoactivity decrease with increasing tungsten content has been recently observed for the same photocatalytic reaction also with a series of TiO_2-WO_3 mixed oxide photocatalysts obtained by coupling TiO_2 with different amounts of WO_3 according to an alkaline-catalyzed sol-gel method followed by an incipient wetting procedure [23].

Conversely, FA photodegradation proceeded at a higher rate with the W-containing photocatalysts of the TW*x*_700 series. TW1_700 was the best performing photocatalyst, in line with previous studies that reported a beneficial effect on titania photoactivity for small amounts

of tungsten [2,3]. This photoactivity trend could be mainly related to the full anatase composition of W-containing samples, along with their larger surface area, resulting from sintering inhibition [3,6], as demonstrated by the d_A values of all photocatalysts collected in Table 1. Among all Ti-W composite materials, independently of the calcination temperature, TW1 exhibit the best performance in FA photo-oxidation, indicating W/Ti = 1 mol% as the optimum molar ratio for photocatalysts prepared under the here adopted conditions. Larger tungsten contents may result in a higher concentration of defect states available for the charge carriers recombination suppressing FA photodegradation rate.

Finally, if the photoactivity of Ti-W mixed oxides with the same nominal tungsten content are compared, those annealed at 700 °C always proved to be better performing than those calcined at 500 °C. This effect, which is even more pronounced for W/Ti = 3 and 5 mol%, very reasonably stems from the higher crystallinity of full anatase TW*x*_700 ensued through high temperature annealing.

3.3. H_2 production through methanol photo-steam reforming

The rates of H_2 production (r_{H2}) by photo-steam reforming of methanol, obtained with all here investigated photocatalysts, are shown in Fig. 3(b). As in previous studies, r_{H2} was evaluated as the slope of the straight lines fitting the amount of hydrogen detected in the gas phase as a function of the irradiation time, normalised per unit catalyst weight [13,24]. Among the materials calcined at 500 °C (the TW*x*_500 series), higher rates of H_2 production were obtained with tungsten-containing photocatalysts, exhibiting higher photoactivity than that of pure anatase TW0_500 (or comparable to, within the experimental error, in the case of TW5_500). Also for TW*x*_700 materials, the presence of tungsten in the photocatalyst led to enhanced H_2 production with respect to that obtained with TW0_700, mirroring the results obtained with these photocatalysts in FA photo-oxidation (Fig. 3(a)). The higher surface areas characterizing all W-

containing materials may play a remarkable role in this gas phase photocatalytic reaction, substrate adsorption notoriously representing a crucial step in heterogeneous catalysis. Furthermore, in the photocatalysts series annealed at 700 °C, the thermal stabilization of the anatase phase induced by the presence of tungsten contributes in increasing the photoactivity of there highly crystalline full anatase materials with respect to TW0_700, which essentially consists of less active rutile phase.

3.4. Electron Paramagnetic Resonance analysis

EPR spectroscopy was used to investigate the fate of photo-promoted electrons, under UV irradiation and in the presence of O_2. The analysis was performed with two photocatalysts calcined at 500 °C, i.e. bare TiO_2 (TW0_500) and TW1_500, which was exemplarily selected as W-containing sample. Fig. 4 shows the EPR signals detected with the two photocatalysts (panels (a) and (b), respectively) and their comparison (panel (c)).

The background EPR signal of pure TiO_2 corresponds to that of nearly stoichiometric TiO_2 (Fig. 4(a), red trace). Upon UV irradiation (black trace), the typical feature corresponding to Ti^{3+} (g = 1.972) is observed due to trapping of photogenerated electrons by Ti^{4+} ions. [25]. Furthermore, due to the presence of molecular oxygen, a fraction of photopromoted electrons is captured by O_2 and the EPR signals of the superoxide radical anion $O_2^{-\cdot}$ (g_{zz} = 2.034, g_{xx} = 2.003) consequently appear . In parallel the photogenerated holes are trapped at oxygen sites and therefore become visible as O^- anions ($g_\perp$ = 2.027, $g_\parallel$ 2.017)in the EPR spectrum. .

The background EPR spectrum of TW1_500 (Fig. 4(b), red trace) shows the presence of traces of nitric oxide (NO) likely trapped in closed cavities within the crystals. In the case of TW1_500 (Fig. 4(b), black trace), upon irradiation with UV light in the presence of O_2, the signals corresponding to oxygen-based paramagnetic species ($O_2^{-\cdot}$and O^- withthe same g values observed for bare titanium dioxide, see above)) are observed. The comparison between the EPR spectra of

TW0_500 and TW1_500, both recorded under UV irradiation and in O_2-atmosphere (Fig. 4(c)), highlights that the EPR signals of all species due to charge carries trapping (Ti^{3+}, O_2^- and O^-) generated in the mixed oxide sample are less intense than those observed for pure titania.

The present EPR results can be discussed in terms of photo-produced holes and electrons that, once generated, can either recombine, be trapped in the bulk or react with species adsorbed on the surface of the semiconductor nanoparticles [26]. In pure titania, in the absence of molecular oxygen, photo-promoted electrons are partly trapped in TiO_2, as corroborated by the presence of the EPR signal due to paramagnetic Ti^{3+} [5,27,28]. However, the electron trapping ability of the oxide is reduced in the presence of O_2, able to scavenge electrons, as proved by the generation of oxygen species, such as O_2^- and H_2O_2, and the consequently decreased accumulation of electrons in the TiO_2 nanoparticles [5,28].

In addition, EPR experiments performed with irradiated TiO_2-WO_3 under *anaerobic* conditions [5] indicate that the majority of photo-promoted electrons are transferred to WO_3, as demonstrated by the largely reduced intensity of Ti^{3+} and O_2^- signals with respect to those detected with pure titania

Although we did not perform EPR measurements at very low temperature (4K), which might have provided us direct evidence of W^{5+} formation under irradiation, we noticed that during H_2 production photocatalytic tests, performed under UV-vis irradiation and in the absence of O_2, all TW*x*_*y* nanopowders (*x* = 1 – 5) assumed a deep blue colour at the end of each catalytic cycle (see inset of Fig. 3(b)) [29], suggesting that under *anaerobic* conditions electrons photo-promoted in TiO_2 can be trapped in W^{5+} form.

3.5. Photocatalytic activity in Ti-W mixed oxides

HAADF-STEM images (Fig. 2) provide evidence that W^{6+} cations are introduced within the hosting TiO_2 lattice. Thus, the electrons photopromoted under irradiation form W^{5+} species [5],

either within the W-doped titania lattice, or by electron transfer from TiO_2 to WO_3 domains on the photocatalyst surface, triggered by the lower WO_3 CB with respect to that of titania (*i.e.*, CB (TiO_2) ~ -0.1 V and CB(WO_3) ~ 0.4 V, both referred to SHE) [30].

Under irradiation in *aerobic* conditions, EPR spectra proved that both Ti^{3+} and $O_2^{-\bullet}$ paramagnetic species were produced to a lower extent in the Ti-W mixed oxides. This finding suggests that, during FA photo-oxidation reactions, photopromoted electrons may either be trapped at W^{5+} sites or be transferred to surface WO_3 domains, but if this occurs, their subsequent transfer to to adsorbed dioxygen would be inhibited [23]. This would result in an increased electron-hole recombination with consequently decreased efficiency in FA oxidation, notoriously proceeding through direct combination of the organic substrate with VB holes [31,32]. In fact, TiW mixed oxides annealed at 500°C were all less efficient than pure titania in FA photo-oxidation (Fig. 3(a), left panel).

The better performance in FA photo-oxidation of TW mixed oxides annealed at 700°C with respect to TW0_700 (Fig. 3(a), right panel) most likely should be ascribed to their full anatase composition and the enhanced specific surface area consequent to the above mentioned stabilization of the anatase phase in the presence of tungsten [6] leading to highly crystalline materials with intrinsically higher photoactivity. Similar effects have been obtained upon addition of small amounts of p-block elements to TiO_2 [33-35].

Similarly, the higher rate of photo-assisted hydrogen production obtained with TiO_2-WO_3 mixed oxides (both TW*x*_500 and TW*x*_700, Fig. 3(b)) can be more likely related to the physico-chemical characteristics of the materials (*e.g.*, full anatase composition, higher crystallinity and specific surface area). In particular, the presence of tungsten led to a decrease in anatase particle dimensions with the consequent increase in the specific surface area of the mixed oxide photocatalysts (Table 1). Higher SSA values together with higher anatase content and samples

crystallinity are often reported to play a remarkable role in enhancing the rate of heterogeneous catalytic reactions, as those occurring at the gas/solid interface [4,36,37].

Of course, W addition may also generate a composite structure in TiO_2 that promotes the electron transfer from excited TiO_2 to WO_3 domains most reasonably localized on the W-doped TiO_2 surface. However, in the case of the presently investigated reactions this would produce a decrease in photactivity due to the lower energy level of the WO_3 CB band, from which electrons cannot efficiently transfer either to O_2 in FA oxidation or to protons to produce H_2 in methanol photosteam reforming.

Furthermore, the introduction of a W excess into the titania lattice might increase the number of electron-hole recombination centers, which negatively affects the photoactivity of the materials. Under present conditions, W/Ti > 1 mol% proved to be negative for the photocatalysts performance, in both oxidation and reduction reactions (Fig. 3). The best performing Ti-W mixed oxide photocatalyst, calcined at 500 or 700 °C, were those containing the lowest W amount, which implies that titania-based mixed oxide photocatalysts with a lattice cell similar to that of TiO_2 (see Fig. 1(b)) ensured the highest photoactivity in the two here investigated reactions. On the other hand, the presence of WO_3 domains on the titania lattice was found to afford better photoactivity in reactions implying a lower laying potential of electron accepting species, such as Cr(VI) reduction [23].

4. Conclusions

Ti/W mixed oxides photocatalysts annealed at 500 °C due to the lower availability of valence band holes due to higher electron-hole recombination due to hampered electron transfer to oxygen in FA photo-oxidation, with respect to pure titania TW0_500. By contrast, the Ti-W composite photocatalysts annealed at 700 °C, due to the beneficial physico-chemical properties ensued by W addition in the TiO_2 lattice (*i.e.*, full anatase composition, enhanced surface area,

higher crystallinity) proved more effective in promoting FA photodegradation, overwhelming electron transfer limitations. Similarly, higher H_2 photoproduction rates were obtained with TiO_2-WO_3 photocatalysts (independently of the annealing temperature) owing to the materials intrinsic properties, rather than to electron transfer and charge separation improvements. Finally, Ti/W = 1 mol% was identified as the optimum mixing ratio, which guarantees minimal distortion of TiO_2 lattice parameters, low concentration of structure defects, full anatase structure even after calcination at 700 °C, yielding always the best photoactivity within the investigated Ti/W mixed oxides.

Acknowledgements

This work received support from the Cariplo Foundation through the 2013-0615 grant to the project *Novel Photocatalytic Materials based on Heterojunctions for Solar Energy Conversion*.

References

[1] M. Dahl, Y. Liu, Y. Yin, *Chem. Rev.* 114 (2014) 9853–

[2] X.Z. Li, F.B. Li, C.L. Yang, W.K. Ge, J. Photochem. Photobiol. A: Chem. 141 (2001) 209–217.

[3] K.K. Akurati, A. Vital, J.P. Dellemann, K. Michalow, T. Graule, D. Ferri, A. Baiker, Appl. Catal. B Environ. 79 (2008) 53–62.

[4] B. Tryba, M. Piszcz, A.W. Morawski, Intern. J. Photoen. (2009) 297319.

[5] D. Zhao, C. Chen, C. Yu, W. Ma, J. Zhao, J. Phys. Chem. C 113 (2009) 13160–13165.

[6] F. Riboni, L.G. Bettini, D.W. Bahnemann, E. Selli, Catal. Today 209 (2013) 28–.

[7] H. Kim, J. Kim, W. Kim, W. Choi, J. Phys. Chem. C 115 (2011) 9797–9805.

[8] T. Ohuchi, T. Miyatake, Y. Hitomi, T. Tanaka, Catal. Today 120 (2007) 233–239.

[9] H. Yang, K. Zhang, R. Shi, A. Tang, J. Am. Ceram. Soc. 90 (2007) 1370–1374.

[10] G. Oskam, A. Nellore, R.L. Penn, P.C. Searson, J. Phys. Chem. B 107 (2003) 1734–1738.

[11] M.V. Dozzi, A. Saccomanni, M. Altomare, E. Selli, Photochem. Photobiol. Sci. 12 (2012) 595–.

[12] M.V. Dozzi, L. Prati, P. Canton, E. Selli, Phys. Chem. Chem. Phys. 11 (2009) 7171–.

[13] G.L. Chiarello, M.H. Aguirre, E. Selli, J. Catal. 273 (2010) 182–.

[14] G.L. Chiarello, D. Ferri, E. Selli, J. Catal. 280 (2011) 168–.

[15] N. Couselo, F.S.García Einschlag, R.J. Candal, M. Jobbágy, J. Phys. Chem. C 112 (2008) 1094–1100.

[16] A.M. Cant, F. Huang, X.L. Zhang, Y. Chen, Y.B. Cheng, R. Amal, Nanoscale 6 (2014) 3875–3880.

[17] R.D. Shannon, Acta Cryst. A 32 (1976) 751–767.

[18] P.P. González-Borrero, F. Sato, A.N. Medina, M.L. Baesso, A.C. Bento, G. Baldissera, C. Persson, G.A. Niklasson, C.G. Granqvist, A. Ferreira Da Silva, Appl. Phys. Lett. 96 (2010) 061909.

[19] M. Carrus, F. Riboni, M. Fantauzzi, A. Rossi, E. Selli, J. van Bokhoven, Appl. Catal. A Gen. 519 (2016) 130–138.

[20] G. Orsini, V. Tricoli, J. Mater. Chem. 21 (2011) 14530–.

[21] C. Bernardini, G. Cappelletti, M.V. Dozzi, E. Selli, J. Photochem. Photobiol. A Chem. 211 (2010) 185–192.

[22] M.V. Dozzi, G.L. Chiarello, E. Selli, J. Adv. Oxid. Technol. 13 (2010) 305–312.

[23] M.V. Dozzi, S. Marzorati, M. Longhi, M. Coduri, L. Artiglia, E. Selli, Appl. Catal. B Environ. 185 (2016) 157–165.

[24] G.L. Chiarello, A. Di Paola, L. Palmisano, E. Selli, Photochem. Photobiol. Sci. 10 (2011) 355–.

[25] S.K. Lee, P.K.J. Robertson, A. Mills, D. McStay, N. Elliott, D. McPhail, Appl. Catal. B Environ. 44 (2003) 173–.

[26] A.L. Linsebigler, G. Lu, J.T. Yates Jr, Chem. Rev. 95 (1995), 735–.

[27] M. Chiesa, M.C. Paganini, S. Livraghi, E. Giamello, Phys. Chem. Chem. Phys. 15 (2013) 9435–.

[28] S. Tatsuma, S. Saitoh, P. Ngaotrakanwiwat, Y. Ohko, A. Fujishima, Langmuir 18 (2002) 7777–.

[29] A. Yamakata, T. Ishibashi, H. Onishi, J. Phys. Chem. B 105 (2001) 7258–.

[30] D.E. Scaife, Sol. Energy 25 (1980) 41–.

[31] Choi

[32] M. Mrowetz, E. Selli, New J. Chem. 30 (2006) 108–114.

[33] M.V. Dozzi, S. Livraghi, E. Giamello, E. Selli, Photochem. Photobiol. Sci. 10 (2011) 343–349.

[34] M.V. Dozzi, B. Ohtani, E. Selli, Phys. Chem. Chem. Phys. 13 (2011) 18217–18227.

[35] M.V. Dozzi, et al. L. Artiglia, G. Granozzi, E. Selli, J. Phys. Chem. C (2015)

[36] L.G. Chiarello, M.V. Dozzi, M. Scavini, J.D. Grunwaldt, E. Selli, Appl. Catal. B Environ. 160-161 (2014) 144–.

[37] G.L. Chiarello, E. Selli, L. Forni, Appl. Catal. B Environ. 84 (2008) 332–.

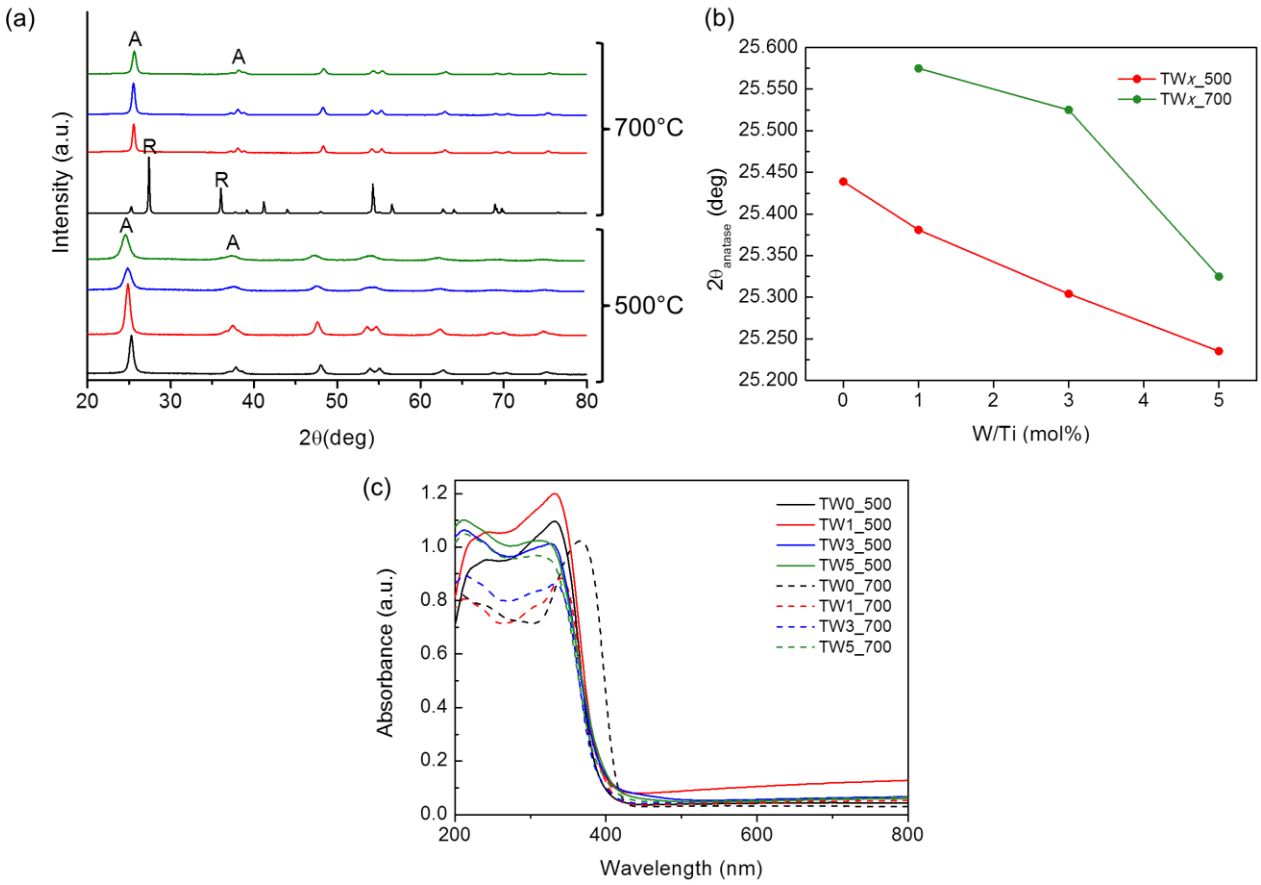

Fig. 1. (a) XRD patterns of pure TiO_2 and of all the W-containing samples, calcined at either 500 °C (bottom) or 700°C (top). A and R indicate the main Anatase and Rutile reflections, respectively. In detail, TW0 (black line), TW1 (red line), TW3 (blue line) and TW5 (green line). (b) Dependence of the 2ϑ-value of the main anatase reflection (*i.e.*, $2\vartheta \sim 25.5°$) on the W content in all the prepared samples. (c) UV-vis absorbance of all the synthesized TW*x* samples, either annealed at 500°C (full lines) or 700°C (dashed lines).

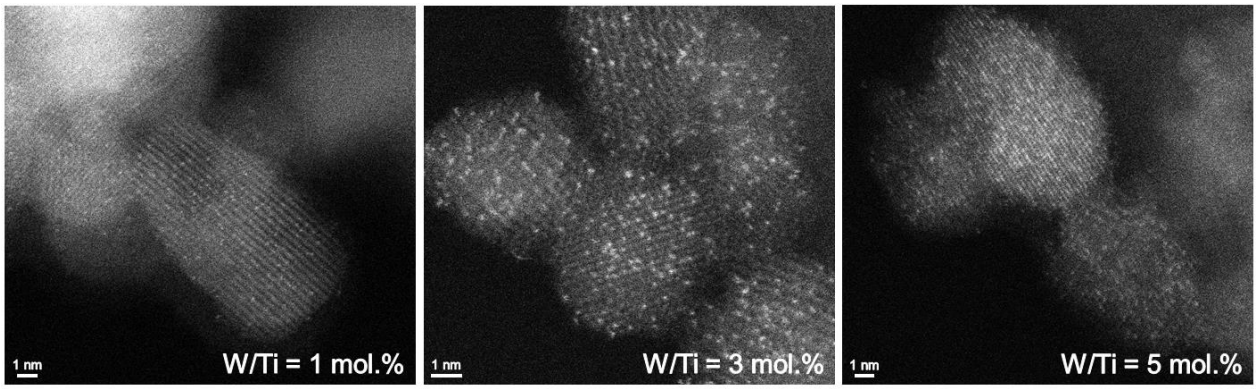

Fig. 2. HAADF-STEM images of the TW1, TW3 and TW5 samples (from left to right), all annealed at 500 °C.

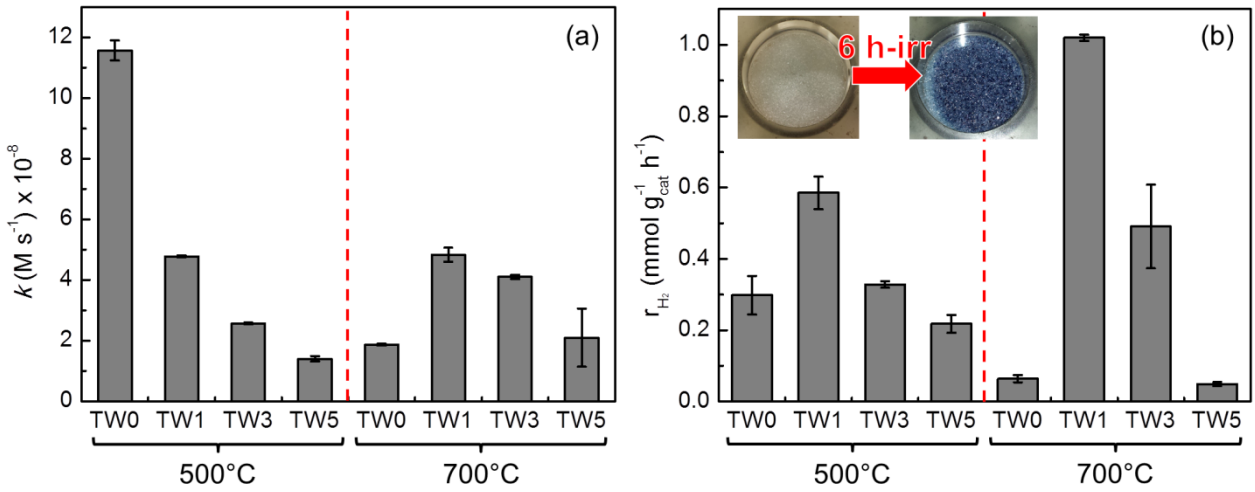

Fig. 3. (a) Zero-order rate constant of formic acid degradation (*k*), obtained with the TW*x*_500 (left) and TW*x*_700 (right) photocatalysts. (b) Comparison of the rate of photocatalytic H_2 production (r_{H2}) obtained with all the investigated photocatalysts, annealed at either 500°C (left) or 700 °C (right). The inset exemplarily shows the powder of the TW1_700 photocatalyst before (left-side) and after (right-side) the 6 h-long kinetic run.

Fig. 4. EPR spectra of: (a) TW0_500, as it is (red trace) and under UV irradiation in O_2-atmosphere (black trace); (b) TW1_500, as it is (red trace) and under UV irradiation in O_2-atmosphere (black trace). (c) Comparison between the EPR spectra of TW0_500 and TW1_500 (black and red traces, respectively), both under UV irradiation in O_2-atmosphere.

Table 1. Anatase particles dimension, d_A, obtained from XRD analysis assuming the absence of amorphous material. Specific Surface Area, SSA, from BET analysis of the synthesized TiO_2 and TiO_2-WO_3 materials.

Sample	d_A (nm)	SSA (m^2 g^{-1})
TW0_500	13	44.6
TW1_500	6	205.8
TW3_500	5	202.2
TW5_500	6	198.2
TW0_700	39	6.7
TW1_700	24	14.8
TW3_700	20	28.7
TW5_700	15	52.9

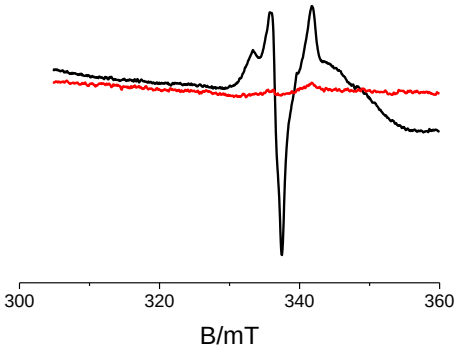
300
320
340
360
B/mT

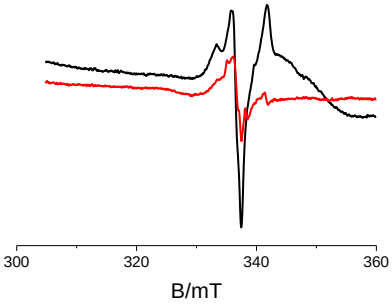
300
320
340
360
B/mT

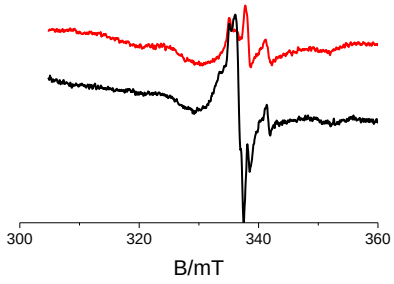
300
320
340
360
B/mT